Catalytic oxidation of 1,2-dichlorobenzene over Ca-doped FeO$_x$ hollow microspheres

Xiaodong Ma [*], Xi Feng, Jie Guo, Huiqin Cao, Xueyue Suo, Hongwen Sun, Meihua Zheng

Key Laboratory of Environmental Pollution Process and Standard, Ministry of Education, Tianjin Key Laboratory of Environmental Remediation and Pollution Control, College of Environmental Science and Engineering, Nankai University, Tianjin 300071, China

ARTICLE INFO

ABSTRACT

Novel Ca-doped FeO$_x$ hollow microspheres were successfully prepared using carbon microspheres as templates. The as-prepared catalysts were characterized by FAAS, XRD, N$_2$ adsorption/desorption, SEM, TEM, H$_2$-TPR and XPS. The catalytic activities of the samples were evaluated by catalytic oxidation of 1,2-dichlorobenzene (*o*-DCB). The results showed that the molar ratios of Ca/(Ca + Fe) in the hollow microspheres and their morphologies significantly affected their catalytic performances. The low-temperature catalytic activity decreased in the order of FeCa10 > FeCa20 > Fe$_2$O$_3$ > FeCa5, in well agreement with the sequence of their reducibility. The optimal FeCa10 catalyst exhibited not only excellent catalytic activity, water-resistant performance and stability but also lower apparent activation energy (21.6 kJ/mol). In situ FTIR measurements revealed the acetate and formate species were the partial oxidation products, which could be subsequently oxidized to form CO$_2$. It is concluded that the excellent catalytic performance of FeCa10 catalyst might be attributed to the combined effects of several factors such as small crystallite size, high surface active oxygen concentration, good low-temperature reducibility and the synergic effect between CaO and Fe$_3$O$_4$. It is reasonable for us to believe that such Ca-doped FeO$_x$ hollow microspheres are promising catalysts for the elimination of chlorinated volatile organic pollutants.

© 2013 Elsevier B.V. All rights reserved.

1. Introduction

Chlorinated volatile organic compounds (Cl-VOCs) produced during municipal solid waste incineration and other combustion processes are considered to be severely harmful to the atmosphere and human health [1–5]. Among the technologies for the removal of Cl-VOCs, catalytic oxidation is thought as the most promising method, due to its lower reaction temperatures, higher destruction efficiencies, and no secondary pollution products are generated [6–9].

The key issue of such a technology is the availability of high-performance catalysts. Noble metal catalysts exhibit excellent catalytic activities for the total oxidation of Cl-VOCs at relatively low reaction temperature, however, high cost, deactivation due to their sensitivity to produced HCl and Cl$_2$, and formation of more toxic substances prohibit their wide applications [10,11]. Alternatively, transition metal oxides are believed to be the optimal catalysts for the total oxidation of Cl-VOCs due to the advantages of lower cost, higher thermal stability and the possibility of fabrication of high-surface area and various morphologies [12–15].

Among transition metal oxides, cheap and environmentally friendly iron oxide catalysts have attracted much attention [16–18]. Further researches have revealed that the Ca-doped iron oxide catalysts exhibited better catalytic activity for the decomposition of Cl-VOCs compared with single iron oxide. It is considered that the higher catalytic activity results from the synergic effect between Fe$_2$O$_3$ and CaO [19–22]. This can be named "Ca-doping effect" of iron oxide in the catalytic oxidation of Cl-VOCs.

It is well known that the morphology and microstructure of catalysts play an important role in the catalytic performance. This is so-called "structure and morphology effect" [23,24]. Recently, iron oxide with different morphologies and nanostructures has been synthesized, including nanoparticles [25], nanowires [26], nanotubes [27], nanorods [28,29], nanoflowers [30] and hollow microspheres [31,32]. Among various nanomaterials, the hollow microspheres with nanometer to micrometer dimensions are of increasing interest for their potential applications in the field of heterogeneous catalysis, due to their low density, high surface area, stability, and surface permeability.

In the past years, a large number of researches have been focused on the above two popular approaches to improve the catalytic activity of iron oxide. However, a combination of the above-mentioned "Ca-doping effect" and "structure and morphology effect", which may further enhance the catalytic performance for the decomposition of Cl-VOCs, has seldom been reported in the literature.

* Corresponding author. Tel.: +86 22 2350 1117; fax: +86 22 2350 1117.
E-mail address: maxd@nankai.edu.cn (X. Ma).

In this paper, Ca-doped FeO_x hollow microspheres have been synthesized by using pre-prepared carbon microsphere as the hard template. The Ca-doped FeO_x hollow microspheres, with the structure and dopant effects, have been systematically examined for the total oxidation of o-DCB, which was used as a model compound of Cl-VOCs. The objectives of this study include: (i) developing a novel, effective, environmentally friendly catalyst for the decomposition of Cl-VOCs, (ii) investigating the effect of the reaction parameters including the reaction temperature and atmosphere on the decomposition efficiency, (iii) examining the structure–reactivity relationship in the light of detailed characterization of the physicochemical properties and the catalytic activities of the catalysts, (iv) studying the stability, reaction kinetics and product selectivity of the optimal catalyst to evaluate the viability of such catalytic systems.

2. Experimental

2.1. Catalyst preparation

All chemicals were of analytical grade and used as received without further purification. Carbon microsphere templates were firstly synthesized as follows: 14 g of glucose was dissolved in 80 mL water to form a clear solution. The solution was then placed in Teflon-sealed autoclave and maintained at 180 °C for 8 h. The samples were then centrifuged, washed by water and ethanol for several cycles, respectively. The obtained carbon spheres were then dried at 60 °C for 12 h under vacuum. To synthesize Ca-doped FeO_x hollow microspheres, 2 g carbon microspheres were uniformly dispersed in 100 ml N,N-dimethylformamide (DMF) by ultrasonication for 1 h. $Fe(NO_3)_3 \cdot 9H_2O$ and $Ca(NO_3)_2 \cdot 4H_2O$ were dissolved in 100 ml DMF solution with suitable ratios, then the salt solution was slowly added to the above mixture and then 60 drops of distilled water were added, followed by ultrasonication for 1 h. The mixed solution was aged under ambient temperature for 24 h. The resulting precursor was centrifugated and washed with distilled water and ethanol, then dried at 80 °C in air for 12 h. Finally, the formed precursor was calcined in air at 500 °C to produce Ca-doped FeO_x hollow microspheres. The nominal content of Ca was 0, 5, 10, and 20 mol%, the corresponding catalysts were denoted as Fe_2O_3, FeCa5, FeCa10 and FeCa20, respectively.

2.2. Catalyst characterization

The chemical compositions of the prepared catalysts were determined by WFX–210 atomic absorption spectroscopy (AAS). For the analysis, the samples were dissolved in 50% HNO_3 solution. The powder X-ray diffraction patterns (XRD) of the samples were recorded on a Rigaku D/max-2500 powder diffractometer using Cu Kα radiation (40 kV and 100 mA). Crystal phases were identified by referring the diffraction lines to those of the powder diffraction files in ICDD-JCPDS database. Nitrogen adsorption/desorption isotherms were collected at 77 K using a Quantachrome NOVA 2000e sorption analyzer after the samples were degassed at 200 °C for 6 h. The specific surface areas were calculated using the multipoint BET (Brunauer–Emmett–Teller) procedure. The pore-size distribution was determined from the desorption branch of the isotherms using the BJH (Barett–Joyner–Halenda) method. Scanning electron microscopy (SEM) images were obtained using a Shimadzu SS-550 apparatus operated at 10 kV. Transmission electron microscopy (TEM) analysis was performed on a TECNAI G^2 F20 microscope, operating at 200 kV. The sample was dispersed in ethanol and treated with ultrasound for 5 min, and then deposited on a copper grid coated with preformed holey carbon film. X-ray photoelectron spectra (XPS) were performed with a Kratos Axis

Ultra DLD spectrometer employing a monochromated Al Kα X-ray source ($h\nu$ = 1,486.6 eV), 150 W, hybrid (magnetic/electrostatic) optics, multi-channel plate and delay line detector. The C 1s signal at binding energy (BE) = 284.6 eV was taken as a reference for BE calibration. Hydrogen temperature-programmed reduction (H_2-TPR) experiments were carried out in the RT-900 °C range on a Thermo-Finnigan TPDRO 1100 instrument with a heating rate of 10 °C/min and a flow rate of 5 vol% H_2/Ar (40 mL/min). Hydrogen consumption was monitored by a thermal conductivity detector. The reduction band was calibrated against that of the complete reduction of a known standard of CuO.

2.3. Catalytic evaluation

Catalytic activity was evaluated at atmospheric pressure in a continuous-flow fixed-bed microreactor. Each run used approximately 50 mg of catalyst in the form of 120–180 mesh particles. A mixture of oxygen/nitrogen (10/90 volume ratio) was divided into two paths, except for the experiment with water, one path flows through a saturator containing o-DCB liquid to carry o-DCB vapor, the other was used as balance gas, The two flows met and mixed in the mixing chamber to get the reaction gas mixture consisting of 50 ppm o-DCB, then the gas mixture was introduced into the catalyst bed at a total flow rate of 60 mL/min. A typical gas hourly space velocity (GHSV) was 88,000 h^{-1}. For measurements in the presence of water, an additional saturator maintained at 40 °C was connected to third path of oxygen/nitrogen stream. Catalytic tests were performed at temperature range of 100–500 °C. After 30 min reaction, o-DCB in the effluent gases was analyzed on-line by a GC1100 gas chromatograph equipped with a flame ionization detector (FID) and a 3.0 m stainless steel column packed with GDX103 (60/80 mesh). The activity was expressed as the conversion of o-DCB, calculated by the following equation:

$$X(\%) = \left(1 - \frac{C_{out}}{C_{in}}\right) \times 100\% \tag{1}$$

where C_{in} is the initial concentration of o-DCB before reaction and C_{out} is the final concentration of o-DCB after reaction. Qualitative analyses of volatile organic products were performed off-line by an Agilent 7890A gas chromatograph equipped with a HP-5MS capillary column (30 m length, 0.25 mm id., 0.25 μm film thickness) and interfaced to Agilent 5973 C MSD in the full scan mode.

2.4. Kinetic studies

To evaluate the kinetics of the catalytic reaction, the mass of the catalyst was fixed at 50 mg, the catalytic activity was investigated in the range of 200–250 °C. The total flow rate of the gaseous mixture flowing through the catalytic reactor was 60 mL/min, the concentration of o-DCB was varied by changing o-DCB flow rate from 0.5 to 2.5 mL/min. Since the concentration of o-DCB was kept at a low level, the amount of heat liberated was very small, and the good cooling system of reaction device let the heat spill out quickly, these conditions can maintain isothermal operation of the reactor.

2.5. In situ FTIR studies

In situ FTIR spectra were recorded using a PerkinElmer 2000 FT-IR spectrophotometer with a resolution of 2 cm^{-1}. The powder samples were compressed into self-supporting thin discs of about 25 mg/cm^2 and 0.1 mm thick. The discs were placed in an IR cell which allowed thermal treatments in vacuum or in a controlled atmosphere. Before each experiment, catalyst samples were pretreated in vacuum at 350 °C for 1 h and then cooled to room temperature or desired temperature, and spectra of the clean catalyst surface were collected and used as the background. In order to
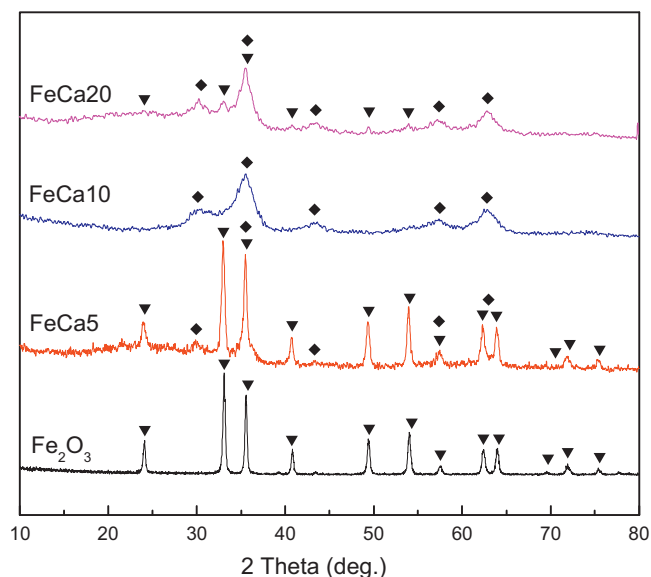
Fig. 1. XRD patterns of the catalysts with different Ca/(Ca + Fe) molar ratios: (▼) α-Fe$_2$O$_3$; (♦) Fe$_3$O$_4$.

investigate the dissociative adsorption of o-DCB on the surface of the catalyst, o-DCB vapor was introduced into the cell in a mixture of 10% O$_2$/N$_2$. In situ FTIR spectra were collected at different time intervals until a steady state was reached.

3. Results and discussion

3.1. Characterization of catalysts

The XRD patterns of the as-prepared catalysts with different Ca/(Ca + Fe) molar ratios are shown in Fig. 1. The chemical composition and main characteristics of the crystalline phases of the synthesized catalysts are listed in Table 1. The pure Fe$_2$O$_3$ hollow microsphere presents only the characteristic reflections of α-Fe$_2$O$_3$ (JCPDS 33-0664). It is known that α-Fe$_2$O$_3$ is the main crystalline phase after calcination at 500 °C. While in this study, Fe$_3$O$_4$ phase (JCPDS 19-0629) appears in all the Ca-doped iron oxide samples, Fe$_3$O$_4$ phase is still stable at such temperature, indicating the crystal structure of FeO$_x$ microspheres has been modified due to the doping of Ca ions. The common crystalline phases of FeCa5 and FeCa20 are α-Fe$_2$O$_3$ and Fe$_3$O$_4$. While for FeCa10, only Fe$_3$O$_4$ phase is observed. The mean crystallite sizes of Fe$_2$O$_3$, FeCa5, FeCa10, FeCa20 and FeCa30 are 32.6, 21.4, 5.3 and 11.5 nm, respectively. Differences in the average particle diameters of the synthesized catalysts can be attributed to the influence of Ca ions with different doping amounts on the crystal structure of iron oxides. No diffraction peaks for any calcium species could be observed in all the catalysts, indicating that calcium species is present in an amorphous form or highly dispersed on the surface of α-Fe$_2$O$_3$ with very small particle sizes. Previous studies have reported that crystal phase of iron oxide can be transited from α-Fe$_2$O$_3$ to Fe$_3$O$_4$ by the cation doping [33]. It is proposed that doped cations induce the formation of oxygen vacancies filled with electrons, which will ionize spontaneously at room temperature, producing conduction-band electrons [e$^-$(cb)], leading to n-type doping of the oxide. If n-doped α-Fe$_2$O$_3$ is placed in contact with water, the electrons will be trapped by surface Fe^{3+} ions, producing Fe^{2+}:

$$e^-(cb) + Fe_s^{3+} \rightleftharpoons Fe_s^{2+} \tag{2}$$

This result leads to the formation of magnetite (Fe$_3$O$_4$). In this case, the doped Ca^{2+} induced the crystalline phase transition
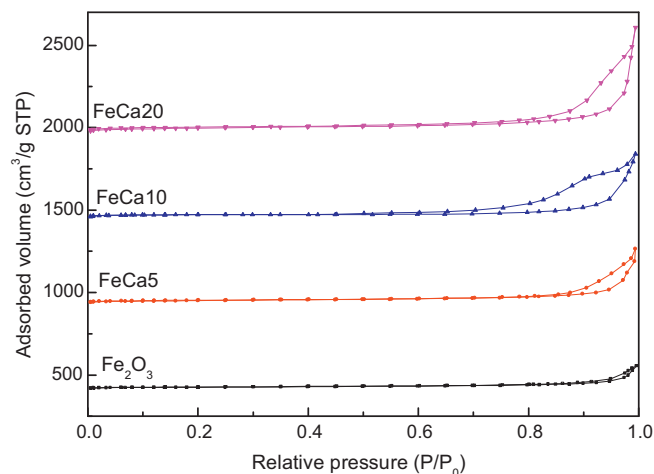

Fig. 2. Nitrogen adsorption/desorption isotherms of the prepared catalysts with different composition.

from α-Fe$_2$O$_3$ to Fe$_3$O$_4$ on the surface of carbon microsphere templates, among which, Fe$_3$O$_4$ nanocrystalline with only 5.3 nm was obtained by the 9.7 mol% Ca-doping.

Fig. 2 depicts the N$_2$ adsorption/desorption isotherms of the synthesized catalysts. All the isotherms are of type IV according to the IUPAC recommendations, which is characteristic of mesoporous materials. The results of specific surface area and volumetric adsorption measurements of the catalysts are listed in Table 1. It can be seen that both specific surface areas and total pore volumes increase with the increase of Ca-doping content. However, average pore diameters present different changing trend, the smallest one was observed in FeCa10 catalyst.

The morphologies of the as-prepared catalysts after calcination were investigated by SEM. The typical SEM images are shown in Fig. 3. It is clear that all the samples exhibit microsphere structure. The pure Fe$_2$O$_3$ hollow microspheres with the average diameter of approximately 430 nm are composed of small nanoparticles with interconnected textural mesopores. Further observation reveals that the Ca doping results in significant change in the structure of the FeO$_x$ microspheres. The sizes of Ca-doped FeO$_x$ hollow microspheres are obviously smaller than those of pure Fe$_2$O$_3$ microspheres, which may be related to the effect of Ca doping on the FeO$_x$ hollow structure. The average diameter of FeCa5, FeCa10 and FeCa20 hollow microspheres are about 220, 140 and 340 nm, respectively. Compared with FeCa5 and FeCa20, FeCa10 exhibits the more intact hollow structure.

The detailed structure features of FeCa10 were further investigated by TEM. A clear contrast between the pale center and dark edge can be observed, conforming the spheres have a hollow interior (Fig. 4a and b). The thickness of the shell is estimated to be about 14.2 nm. The high-resolution TEM (HRTEM) image shown in Fig. 4c reveals the interplanar spacing of 0.25 nm for the (3 1 1) plane of Fe$_3$O$_4$ nanoparticles. The energy-dispersive X-ray spectrometry (EDS) result from Fig. 4d confirms the coexistence of Ca and Fe elements on the surface of FeCa10 catalyst.

The surface element composition, element oxidation state, and adsorbed species of the catalysts were measured by X-ray photoelectron spectroscopy (XPS). Fig. 5a illustrates the high-resolution XPS spectra of Ca 2p from the Ca-doped FeO$_x$ hollow microspheres. The peaks located at 346.6–347.2 and 349.8–350.7 eV can be attributed to Ca 2p$_{3/2}$ and Ca 2p$_{1/2}$ of CaO, respectively [34,35]. It is noteworthy that Ca content on the surface is lower than that of the bulk, and the surface Ca content does not continuously increase with the rise of bulk Ca content. The highest surface Ca content (5.6%) is obtained on the surface of FeCa10 catalyst.

Table 1
Surface element compositions, specific surface areas, crystal phases and the results of volumetric adsorption measurements of the prepared catalysts with different composition.

	Ca/(Ca + Fe) (%)	S_{BET}[a] (m²/g)	V_p[b] (cm³/g)	D_p[c] (nm)	Crystalline species		Crystallite size (nm)
Fe₂O₃	0	73.2	0.23	17.7	α-Fe₂O₃		32.6[d]
FeCa5	4.8	77.2	0.51	31.4	α-Fe₂O₃	Fe₃O₄	21.4[d]
FeCa10	9.7	78.7	0.61	16.1		Fe₃O₄	5.3[e]
FeCa20	19.9	134.0	0.99	28.7	α-Fe₂O₃	Fe₃O₄	11.5[e]

[a] BET specific surface areas.
[b] Total pore volumes.
[c] Average pore diameters.
[d] Calculated from line broadening of α-Fe₂O₃ (1 0 4) by the Scherrer equation.
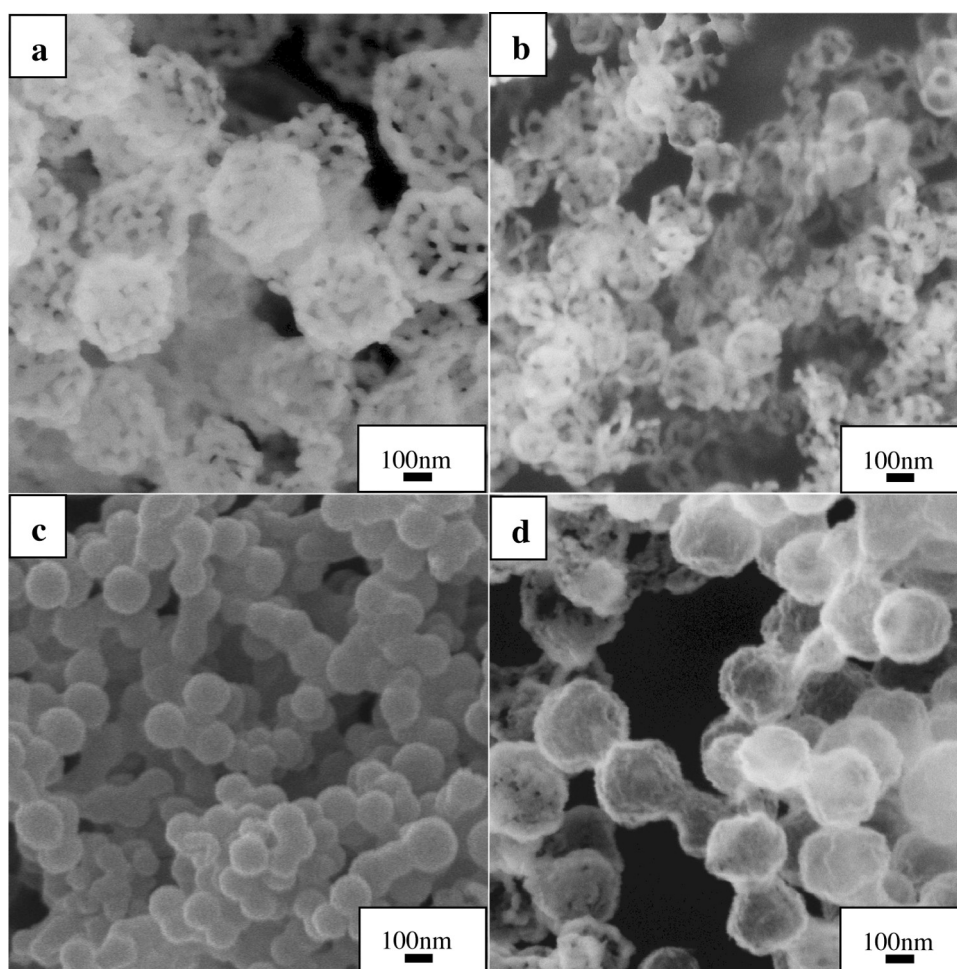[e] Calculated from line broadening of Fe₃O₄ (3 1 1) by the Scherrer equation.

Fig. 3. SEM images of (a) Fe₂O₃, (b) FeCa5, (c) FeCa10 and (d) FeCa20.

Fig. 5b and c illustrate the Fe $2p_{3/2}$ and O 1s XPS spectra of the catalysts, respectively. As shown in Fig. 5b, the asymmetrical Fe $2p_{3/2}$ signal of the composite catalysts can be deconvoluted to two components: one at 710–7–712.3 eV and the other at 710.2 eV [36,37]; the former is attributed to surface Fe^{3+}, whereas the latter is attributed to surface Fe^{2+}. Surface Fe^{3+}/Fe^{2+} molar ratios can be obtained by the quantitative analysis on the Fe $2p_{3/2}$ XPS spectra, the results are summarized in Table 2. It can be seen that the Fe^{3+}/Fe^{2+} molar ratio has a close relationship with the Ca content on the surface of the catalyst. The higher surface Ca content, the

Table 2
XPS results of the prepared catalysts with different composition.

Catalyst	Fe%	Ca%	O%	Fe $2p_{3/2}$ (eV)		O 1s (eV)			Fe^{3+}/Fe^{2+}	$O_{sur}/(O_{latt} + O_{sur} + O_{ads})$
				Fe^{3+}	Fe^{2+}	O_{latt}	O_{sur}	O_{ads}		
Fe₂O₃	31.4	0	68.6	710.7		530.5	531.7	534.0	∞	0.32
FeCa5	32.2	2.4	65.4	711.0	710.2	529.8	531.6	533.4	4.13	0.25
FeCa10	29.8	5.6	64.6	712.3	710.2	529.6	531.7	533.6	2.01	0.57
FeCa20	31.3	4.3	64.4	711.3	710.2	529.8	531.1	533.2	2.70	0.27

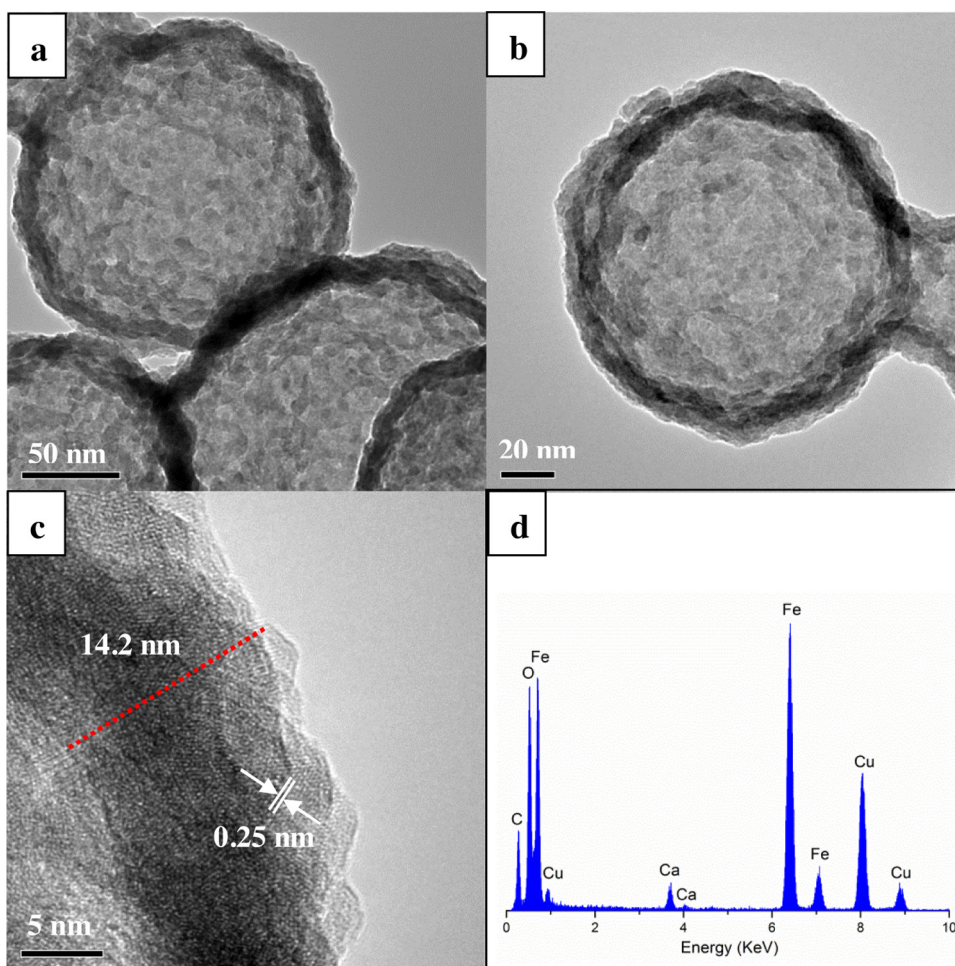**Fig. 4.** (a and b) Typical TEM images, (c) HRTEM image of FeCa10, and (d) EDS spectrum of FeCa10 shown in (c).

lower surface Fe^{3+}/Fe^{2+} molar ratio. FeCa10 with the highest surface Ca content shows the lowest surface Fe^{3+}/Fe^{2+} molar ratio (2.01), which is in close to the theoretical value of pure Fe_3O_4.

As can be seen from Fig. 5c, the asymmetrical O 1s signal of the catalysts could be deconvoluted to three components: lattice oxygen (O_{latt}) at 529–530 eV, surface active oxygen (O_{sur}) at 531–532 eV and adsorbed oxygen species (O_{ads}) at 533–534 eV [38]. It is found from Table 2 that $O_{sur}/(O_{latt} + O_{sur} + O_{ads})$ molar ratios of the catalysts decreased in the order of FeCa10 (0.57) > Fe_2O_3 (0.32) > FeCa20 (0.27) > FeCa5 (0.25). Obviously, the 9.7 mol% Ca-doping leads to the highest O_{sur} concentration. It is known that the higher O_{sur} concentration, the better the catalytic activity [14]. This may give another reasonable explanation for the high activity of FeCa10 in the following activity measurements.

The reducibility of as-prepared catalysts was evaluated by H_2-TPR. The results are shown in Fig. 6. Fig. 6a illustrates the H_2-TPR profiles of all the samples. For Fe_2O_3, FeCa5 and FeCa20 sample, there are obvious reduction peak at 369, 375 and 396 °C, respectively, corresponding to reduction of Fe_2O_3 to Fe_3O_4 [16,39,40]. A broad band centered at 320 °C for FeCa10 sample was observed, which could be attributed to the initial reduction step of very small Fe_3O_4 particles. Similar size-dependent reducibility has been reported in previous work [11].

To further compare the low-temperature reducibility of the prepared catalysts, we calculated the initial H_2 consumption rate per gram of a material before the occurrence of phase transformation (where the initial H_2 consumption of the first reduction peak of each catalyst is less than 25%) [14], as shown in Fig. 6b. It is clear that the initial H_2 consumption rate decreases in the following order: FeCa10 > FeCa20 > Fe_2O_3 > FeCa5. It could be deduced that the low-temperature reducibility of prepared catalysts coincide with the above order.

3.2. Activity measurements

Fig. 7a shows catalytic performance for o-DCB oxidation over commercial Fe_2O_3 (C-Fe_2O_3) and as-prepared hollow microspheres without water vapor. It is noted that all the o-DCB conversion first increases, then decreases, and finally starts to increase again. The first increase and decrease of o-DCB conversion could be mainly attributed to the adsorption and thermal desorption of o-DCB, respectively. The second increase of o-DCB conversion could be ascribed to the oxidation degradation of o-DCB. Similar catalytic behavior has also been reported in the catalytic oxidation of chlorobenzene over MnO_x-CeO_2 catalysts [11].

It can be seen that as-prepared hollow microspheres, except FeCa5, are significantly superior to commercial Fe_2O_3 in the catalytic performance. For pure Fe_2O_3 hollow microsphere, o-DCB conversion is 85.7% at 350 °C, which is almost 50% higher than that of C-Fe_2O_3. The total conversion of o-DCB over Fe_2O_3 hollow microsphere can be obtained at 450 °C. However, the Fe_2O_3 catalyst has a lower catalytic activity in the low temperature range from 200 to 300 °C, for instance, only 28.9% o-DCB conversion at 250 °C.

The catalytic performance of the FeO_x hollow microspheres in the low temperature range can be significantly improved by doping appropriate amount of Ca. In the temperature range
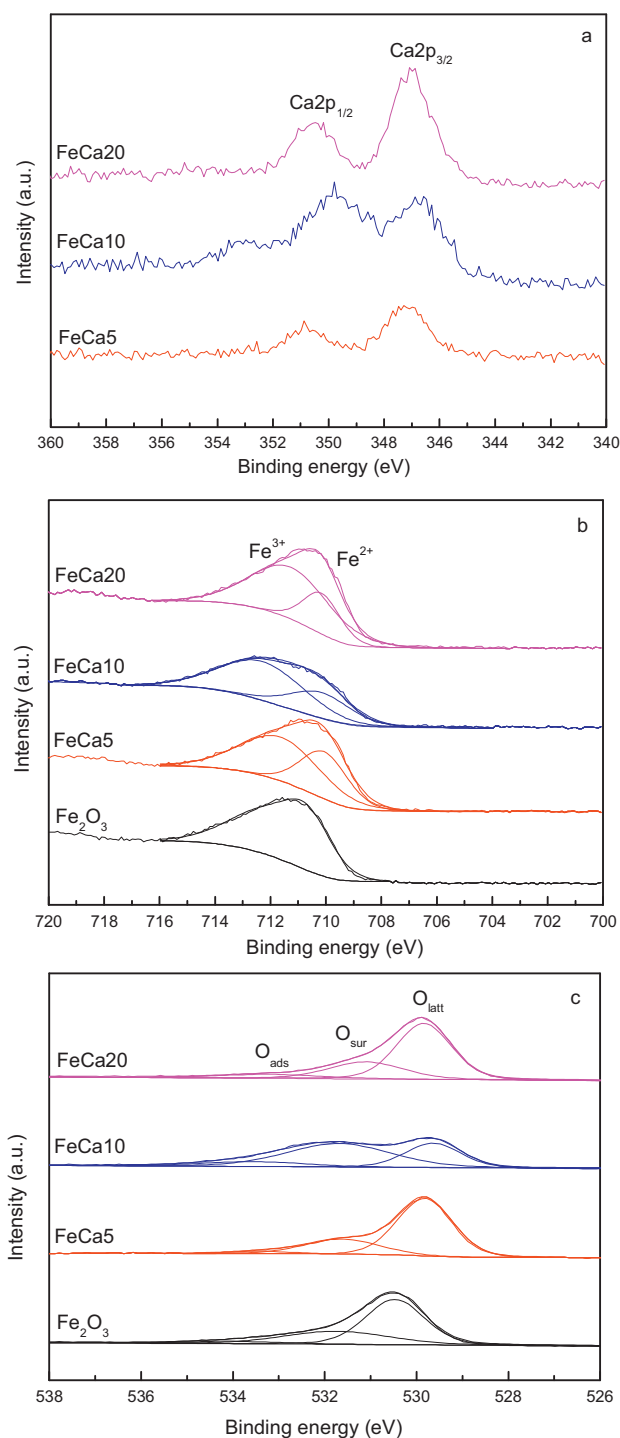
Fig. 5. (a) Ca 2p XPS spectra of Ca-doped FeO$_x$ hollow microspheres, (b) Fe2p$_{3/2}$ and (c) O$_{1s}$ XPS spectra of prepared hollow microspheres.

Fig. 6. (a) H$_2$-TPR profiles and (b) initial H$_2$ consumption rates of prepared hollow microspheres.

of 200–300 °C, the catalytic activity decreases in the order of FeCa10 > FeCa20 > Fe$_2$O$_3$ > FeCa5, coinciding with the sequences of low-temperature reducibility obtained by H$_2$-TPR studies. It is noted that the catalytic activity of Fe$_2$O$_3$ hollow microsphere increases faster than the other catalysts with the rise of temperature, which leads to the change of activity order at elevated temperatures, for example, when reaction temperature is above 350 °C, the catalytic activity decreases in the order of FeCa10 > Fe$_2$O$_3$ > FeCa20 > FeCa5, being in accordance with the sequences of active oxygen species concentration. Such a
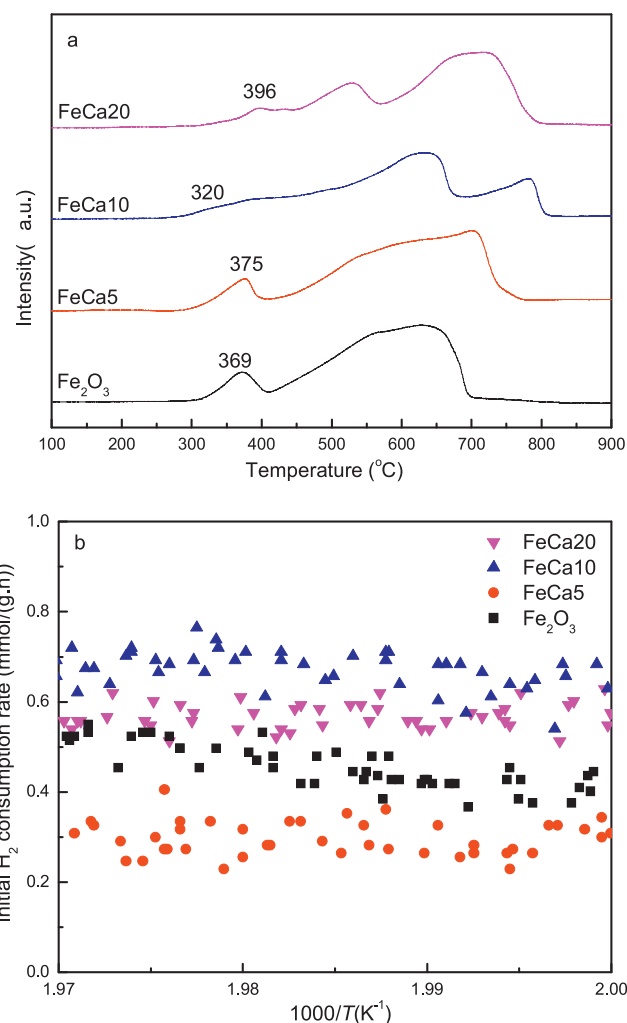
phenomenon might be related to the nature and distribution of active oxygen species (O$^-$, O$_2^-$ and O$_2^{2-}$) on the Fe$_2$O$_3$ surface. It is known that active oxygen species can be converted from O$_2^-$ (the lowest activity) to O$^-$ (the highest activity) with the increase of temperature [14]. Although Fe$_2$O$_3$ possesses more active oxygen species than FeCa20 and FeCa5, the O$^-$ concentration might be lower on the surface of Fe$_2$O$_3$ at lower temperatures, leading to the lower activity of Fe$_2$O$_3$ at lower temperatures. A larger amount of O$^-$ might be formed with the rise of temperature, resulting in the improvement of catalytic activity. Among all the catalysts, FeCa10 with 9.7 mol% Ca-doping exerts the best catalytic activity. At 250 °C, o-DCB conversion is 31.8% higher than pure Fe$_2$O$_3$, up to 60.7%. The total conversion temperature of o-DCB over FeCa10 was obtained at 400 °C. In the previous work, we have reported the catalytic oxidation of o-DCB over CaCO$_3$/α-Fe$_2$O$_3$ nanocomposites [15], over which the total conversion of o-DCB could be obtained at 450 °C under the GHSV of 22,000 h^{-1}. Interestingly, compared with the CaCO$_3$/α-Fe$_2$O$_3$ nanocomposites, the total conversion temperature of o-DCB is 400 °C, even under the higher GHSV of 88,000 h^{-1}, which indicates that the current FeCa10 hollow microsphere exhibits higher catalytic activity.

The high activity of FeCa10 could be attributed to its special composition and structure. The XRD characterization results show that the FeCa10 hollow microsphere is composed of Fe$_3$O$_4$ nanocrystalline. Fe$_3$O$_4$ is a ferrite containing a cubic inverse spinel structure
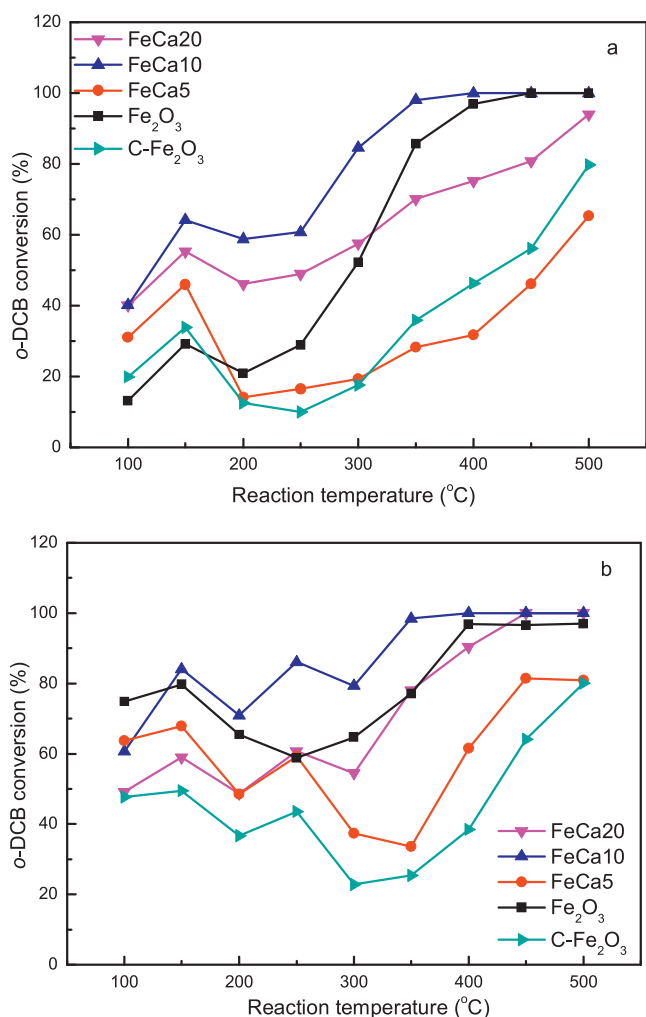
Fig. 7. Light-off curves for the oxidation of *o*-DCB over different catalysts (a) in the absence of water and (b) in the presence of 0.5% water (50 ppm *o*-DCB, 10% O_2, balance N_2, GHSV = 88,000 h^{-1}, time on stream = 5 h).

catalytic properties are attributed to the Cl^-/O^{2-} exchange between the CaO and $FeCl_3$, the latter are formed during the reaction of Fe_2O_3 with chlorinated hydrocarbons. As a result, Cl^- are transferred into calcium oxide, regenerating Fe_2O_3 [19]. In our case, Fe_3O_4 nanocrystallines with smaller crystallite sizes constitute the hollow microspheres, on the surface of which highly dispersed CaO keeps in an intimate contact with Fe_3O_4. This unique structure is more favorable for the strong interaction between the two active phases and facilitates Cl^- exchange between CaO and the formed $FeCl_3$. Amorphous or highly dispersed CaO finally serves as a sink for Cl^-, leading to the formation of $CaCl_2$. The ideal reaction can be described with the following equations:

$$2FeCl_3 + 3CaO = Fe_2O_3 + 3CaCl_2 \tag{3}$$
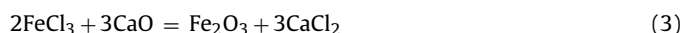
For the catalytic oxidation of Cl-VOCs, it is generally believed that the catalyst with a higher surface area would show a better catalytic activity [44]. While in this case, the catalytic activity of the prepared catalysts was not always associated with the increase of the specific surface area. It can be seen in Table 1 that the specific surface area of FeCa20 was much higher than that of FeCa10, but its catalytic activity was inferior to FeCa10. This result indicates that specific surface area was a minor factor influencing the catalytic activity. From the above results, it can be concluded that compared with FeCa20, the high activity of FeCa10 was mainly related to small crystallite size, high surface active oxygen concentration and good low-temperature reducibility.

The light-off curves for the oxidation of *o*-DCB over commercial Fe_2O_3 catalyst and as-prepared hollow microspheres in the presence of 0.5% water are shown in Fig. 7b. Obviously, when water is present, all the prepared catalysts show higher catalytic activities than commercial Fe_2O_3. In the temperature of 100–200 °C, the light-off curves of prepared hollow microspheres, except pure Fe_2O_3, show the tendency of first rise then fall, which is similar to that in the dry reaction. The difference is that the higher initial *o*-DCB conversion is observed when water is added. However, in the following process, the light-off curves show significantly different characteristics compared with the dry conditions. The light-off curves do not increase continuously with the further rise of the reaction temperature, but increase, with a local maximum conversion (at 250 °C), then decreases with a local minimum (at 300 °C, except FeCa5 at 350 °C), finally increases again with rising temperature. These results indicate that the presence of water during the oxidation of *o*-DCB over Fe-based catalysts results in different catalytic behavior depending on the reaction temperature. Similar phenomenon has also been reported in the oxidation of dichlorobenzene over V_2O_5/TiO_2 [45]. The light-off curve of pure Fe_2O_3 hollow microsphere is obviously different from the other catalysts when water is present. The *o*-DCB conversion firstly increases gradually, thereafter decreases again at temperatures above 150 °C, the minimum of *o*-DCB conversion also appears at 250 °C, then increases again at temperature above 250 °C. It can be seen that water should have different effects on the *o*-DCB conversion over different catalysts, which could be related to different nature of various catalysts.

Previous studies have shown that water has a complicated effect on the performance of catalytic oxidation of Cl-VOCs over metal oxide catalysts. Poplawski et al. [46] reported that water had a promoting effect on the oxidation of *o*-DCB over ABO_3-type perovskites. In the oxidation of *o*-DCB over Co_3O_4/TiO_2, similar promoting effect has been also reported by Krishnamoorthy et al. [47]. In contrast, Albonetti et al. [12] and Krishnamoorthy et al. [47] reported that water could lead to the deactivation of V_2O_5- and Cr_2O_5-based catalysts during the oxidation of dichlorobenzene. Hetrick et al. [45] observed a bimodal activation/deactivation behavior of water during *m*-dichlorobenzene oxidation over a
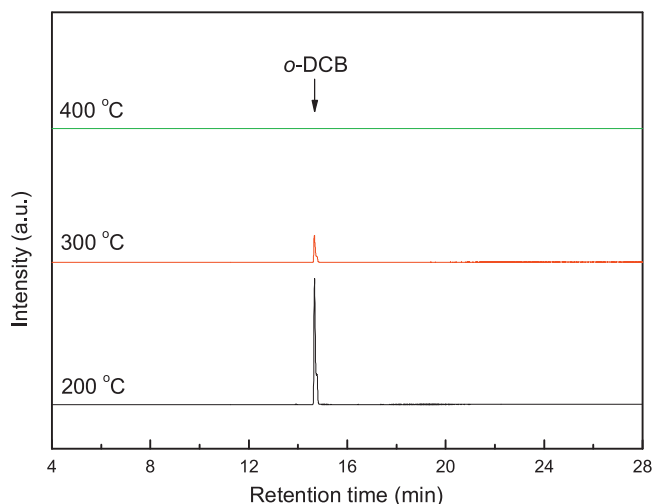
with oxygen anions forming a face-center-cubic (FCC) closed packing and Fe cations occupying both the interstitial tetrahedral and octahedral sites [41]. The high catalytic activity of Fe_3O_4 resulting from its unique structure has been proven by many researches [40,42]. The unique structure of Fe_3O_4 can readily undergo rapid electron exchange between Fe^{3+} and Fe^{2+}. The electron hopping between Fe^{3+} and Fe^{2+} can facilitate the redox reaction [40,42].

Besides, the high activity of FeCa10 is also associated with smaller crystallite size of Fe_3O_4 nanoparticles, which are assembled into hollow structure. Size-dependent catalytic activity has been reported in the previous studies. It is known that smaller crystallite size means more crystalline defects, more active surface sites and higher catalytic activity [43].

Another remarkable structure characteristic of FeCa10 is the high concentration of active oxygen species (O_{sur}) on the surface. The O_{sur} concentration on FeCa10 is up to 57%, which is the highest among all the Ca-doped FeO_x hollow microspheres. It has been proved that high proportion of surface oxygen species on the catalyst means better catalytic activity [11]. The results of XPS quantitative analyses show that surface Ca content on FeCa10 is the highest (5.6%) among all the Ca-doped FeO_x hollow microspheres. XRD results suggest that amorphous or highly dispersed CaO could be present on the surface of FeCa10. Previous studies have indicated that CaO can significantly improve the dechlorination and oxidative properties of Fe_2O_3 [19–22]. These improvements of

Fig. 8. Chromatograms of volatile organic products after o-DCB decomposition over FeCa10 at 200, 300 and 400 °C.

Fig. 9. The effect of oxygen concentration on the activity of FeCa10 (50 ppm o-DCB, 10% O_2, balance N_2, GHSV = 88,000 h^{-1}, time on stream = 5 h).

V_2O_5/TiO_2 catalyst, which depended on reaction temperature. At lower reaction temperatures (<270 °C), the addition of water results in a higher m-dichlorobenzene conversion than the dry reaction. In contrast, at higher reaction temperatures (>350 °C), the presence of water results in the deactivation of the catalyst. In this case, when water is introduced into the feed stream, o-DCB conversions are higher than the corresponding ones for dry oxidation in the temperature range of 100–250 °C. This phenomenon is similar to previous literature reports regarding the behavior of V_2O_5/TiO_2 catalysts [45]. The promoting effect of water in this stage might result from the surface activation assisted by water through Cl and C removal [45], which leads to the exposure of more fresh active sites. Compared with the dry reaction, when water is added, an obvious change in the light-off curves of Ca-doped hollow microspheres is that the catalytic activities are inhibited at 300 or 350 °C. Similar results have been reported in the catalytic oxidation of o-DCB over $CaCO_3/\alpha$-Fe_2O_3 [15], which could be attributed to the competitive adsorption of water on the active sites of the catalysts at an intermediate temperature [45]. As shown in Fig. 7b, when water is present, FeCa10 is also the most active catalyst, although the slight reduction of o-DCB conversion appears at 300 °C, o-DCB conversions over FeCa10 are generally higher than the corresponding ones at different temperatures without water, indicating the high water-resistant performance of FeCa10 catalyst.

Volatile organic products after o-DCB decomposition over FeCa10 at different temperatures in the absence of water were qualitatively analyzed by gas chromatography-mass spectrometry in the full scan mode. The chromatograms are shown in Fig. 8. It can be seen that the peak of o-DCB becomes weak with the increase of reaction temperature and disappears after reaction at 400 °C. It is noteworthy that no other volatile organic products are detected except o-DCB, suggesting the high degree of mineralization of o-DCB has been achieved over the FeCa10 hollow microspheres.

3.3. Effect of oxygen concentration on o-DCB conversion

In order to investigate the effect of O_2 concentration on the conversion of o-DCB over FeCa10 catalyst, O_2 concentration is changed from 0% to 20%, with o-DCB concentration maintained at 50 ppm, the results are shown in Fig. 9. It can be seen that the conversion of o-DCB takes place even in the absence of gas-phase oxygen, indicating that surface lattice oxygen of the catalyst is likely involved in the o-DCB oxidation. However, when 10% O_2 is present in the feed, the relatively higher o-DCB conversion is observed, the total
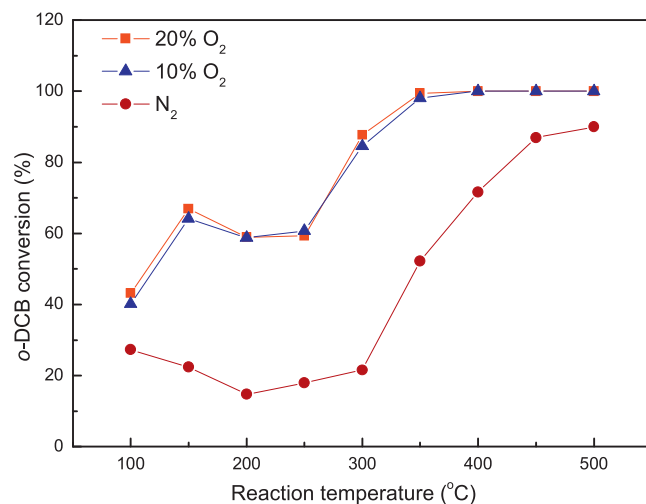
conversion rate of o-DCB is reached at 400 °C, while the value is only 71.6% without O_2. This suggests that O_2 should play an important role in the catalytic oxidation of o-DCB. The further investigation discovers that relatively small amounts of O_2 (i.e. up to 10%) are sufficient for the conversion of o-DCB, therefore, the presence of additional amounts of O_2 (i.e. up to 20%) in the feed does not have further promoting effect. We can deduce from the above discussion that O_2 molecular can not directly take part in the catalytic oxidation of o-DCB but firstly activate or regenerate the active oxygen species located in the vacancies of the catalysts. The amounts of active oxygen species might be restricted by vacancy concentration, and could not continuously increase with the rise of O_2 concentration. This could give a reasonable explanation why excessive O_2 has little effect on the catalytic activity of the catalyst.

Based on the results in this study and previous work, it could be deduced that the catalytic oxidation of o-DCB over FeCa10 follows the Mars-van Krevelen mechanism. It is generally believed that vacancies bind adsorbates more strongly than normal oxide sites and assist in their participation in the catalytic reaction. Firstly, o-DCB is oxided by active oxygen species adsorbed at the surface oxygen vacancies, active oxygen species is reduced. Secondly, the consumed active oxygen species is replenished by the O_2 molecular. In this redox process, appropriate amount of oxygen is beneficial for the activation of active oxygen and improvement of the catalytic activity.

3.4. Catalyst stability

For practical use, it is very necessary to investigate the stability of the catalyst. In previous work, deactivation of the catalysts in the catalytic oxidation of Cl-VOCs has been reported. For example, Liu et al. [48] found that chlorobenzene conversion over MnO_x/TiO_2 catalyst rapidly dropped by about 30% after continuous reaction for 10 h at 400 °C. Wang et al. [18] discovered that iron oxide exhibited better catalytic stability than manganese oxide in the catalytic oxidation of chlorobenzene.

In this study, the stability test results of Fe_2O_3 and FeCa10 for the catalytic oxidation of o-DCB are presented in Fig. 10. It can be seen that the both FeCa10 and Fe_2O_3 keep high stability even after continuous reaction for 750 min without water, with o-DCB conversion being 92.9% and 87.9%, respectively. The higher stabilities of Fe_2O_3 and FeCa10 may be related to their unique hollow structures. Compared with Fe_2O_3, FeCa10 shows higher stability after long-term test, which could be attributed to the Ca-doping effect.
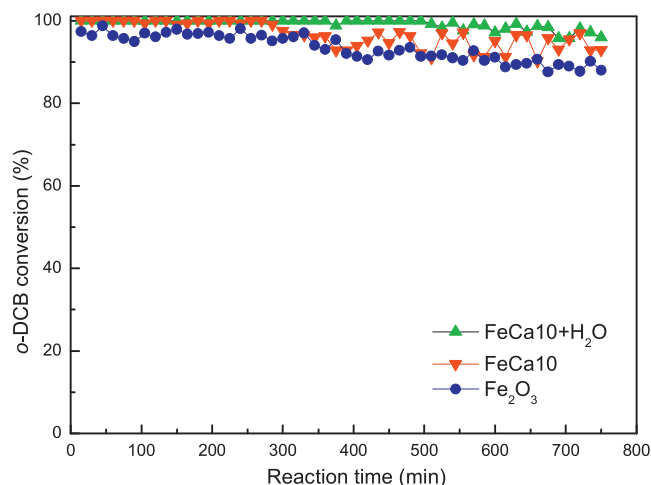
Fig. 10. The stability tests of Fe_2O_3 and FeCa10 hollow microspheres at 400 °C (50 ppm o-DCB, 10% O_2, balance N_2, GHSV = 88,000 h^{-1}).

As discussed above, Ca species can improve the Cl^- exchange and regenerate the active sites on the iron oxide, which is beneficial for keeping the catalytic stability.

It is clearly noted that the introduction of water into the reaction atmosphere does not inhibit, but further improve the catalytic activity and stability of FeCa10. When water is present, the o-DCB conversion over FeCa10 maintains at 95.9% after reaction for 750 min, which is superior to that in the dry reaction. This might result from the removal of adsorbed Cl^- or residual carbonaceous species on the surface of FeCa10 by water. Although the removal of residual Cl^- and carbonaceous species from the surface of used catalysts is known as a slow step, o-DCB conversion over FeCa10 still maintains a high level even after long-time reaction. This could be attributed to the unique Ca-doped hollow structure of FeCa10, which is beneficial for the rapid removal of the Cl^- or carbonaceous species on the surface.

To investigate the change in the species on the FeCa10 surface after reaction, the used FeCa10 (in the presence of water) was analyzed by XPS. No obvious residual carbonaceous species on the surface of FeCa10 was detected. While O1s and Cl 2p XPS spectra of the used FeCa10 exhibit different characteristics in Fig. 11, compared with those of the fresh catalyst. It can be seen from Fig. 11a that, after reaction, peaks of O_{latt}, O_{sur} and O_{ads} shift from 529.6, 531.7 and 533.6 to 529.7, 531.8 and 533.1 eV, respectively. The $O_{sur}/(O_{latt} + O_{sur} + O_{ads})$ molar ratios of FeCa10 decreases from 0.57 to 0.21, confirming that surface active oxygen species takes part in the catalytic oxidation of o-DCB and is consumed after a long-time reaction. Cl 2p peak at 198.2 eV is observed on the XPS spectrum of the used FeCa10 catalyst (Fig. 11b), indicating the presence of Cl^- on the used FeCa10 catalyst. The amount of deposited Cl^- is about 5.0% estimated by XPS. It is known that HCl and Cl_2 are the possible products during the process of catalytic oxidation of Cl-VOCs. Considering the water exists in the feed stream in this study, it is reasonable to deduce that the HCl is the predominant chlorine-containing product in the effluent stream. Similar results have been reported in the previous work [49–52].

3.5. Kinetic studies

Considering the best catalytic activity of FeCa10, the kinetics of catalytic oxidation of o-DCB over FeCa10 was investigated. The results are shown in Fig. 12.
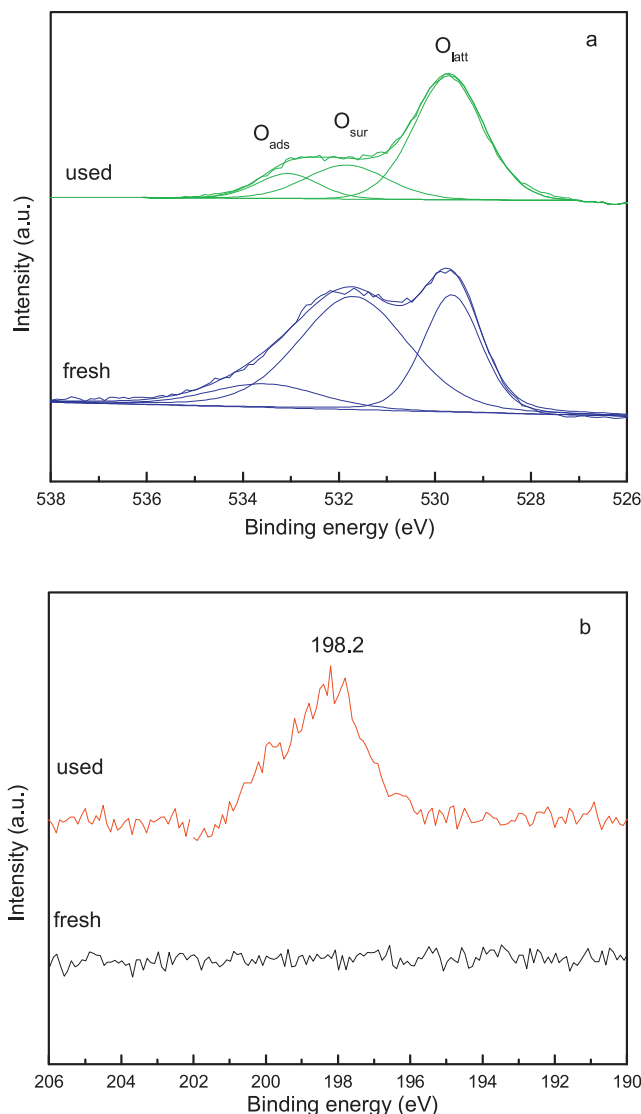

Fig. 11. (a) O1s and (b) Cl 2p XPS spectra of the fresh and used (in the presence of 0.5% water) FeCa10 hollow microsphere (50 ppm o-DCB, 10% O_2, balance N_2, GHSV = 88,000 h^{-1}).
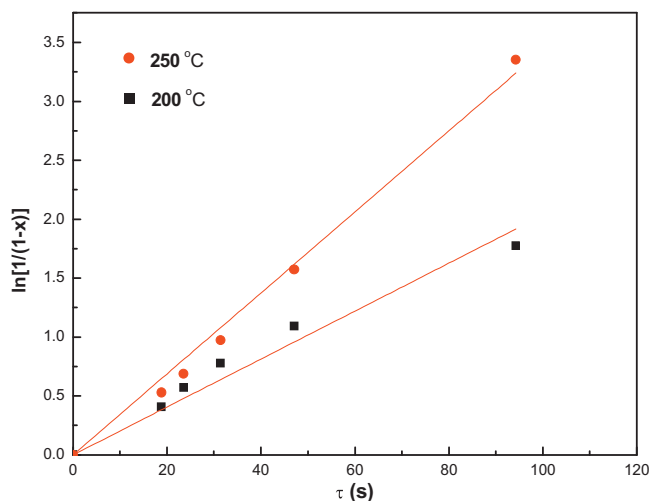

Fig. 12. Plots of $\ln[1/(1-X)]$ vs. space time (τ) at different temperatures using FeCa10 (50 ppm o-DCB, 10% O_2, balance N_2, GHSV = 88,000 h^{-1}).

The rate of catalytic oxidation of o-DCB, r, can be represented by the following equation:

$$r = -\frac{d[CB]}{dt} = k[CB]^m[O_2]^n \tag{4}$$

where [CB] and [O2] are the concentration of o-DCB and O2, respectively. k is the apparent rate constant of the reaction. Since $[O_2] \gg [CB]$, Eq. (4) can be rewritten as follows:

$$r = -\frac{d[CB]}{dt} = k_{ap}[CB]^m \tag{5}$$

Suppose this reaction obeys a first-order rate law, in terms of Eq. (1), Eq. (5) can also be written as:(6)$\ln\left[\frac{1}{1-X}\right] = k'_{ap}\tau$where$\tau$ is the space time (s), and is defined as the reciprocal of the space velocity. Fig. 12 shows the plot of $\ln[1/(1 - X)]$ versusτ for the catalytic oxidation of o-DCB over FeCa10 catalyst with the correlation coefficient (R^2) of 0.985 and 0.995 at 200 and 250 °C, respectively. The results indicate a straight-line relationship between $\ln[1/(1-X)]$ andτ, supporting the assumption that catalytic oxidation of o-DCB is first-order reaction [53]. A straight line plot of $\ln[1/(1 - X)]$ versusτ yields the slope of $k_{ap'}$. The apparent rate constants of o-DCB conversion at 473 and 523 K are $k'_{ap1} = 0.02034\,s^{-1}$ and $k'_{ap1} = 0.03436\,s^{-1}$, respectively. According to the Arrhenius equation (Eq. (7)), the apparent activation energy of the catalytic oxidation of o-DCB over FeCa10 was calculated to be about 21.6 kJ/mol.

$$\ln\frac{k'_{ap1}}{k'_{ap2}} = \frac{E_a}{R}\left(\frac{1}{T_2} - \frac{1}{T_1}\right) \tag{7}$$

where k'_{ap1} and k'_{ap2} are the apparent rate constants at 473 and 523 K, respectively, s^{-1}; E_a is the apparent activation energy, kJ/mol; and T_1 and T_2 are the reaction temperatures, K. The apparent activation energy in this study is significantly lower than those in the catalytic oxidation of 1,2,4-trichlorobenzene (27 kJ/mol) over Co_3O_4–CeO_2 composite oxide in the temperature range of 300–400 °C [9], 1,2-dichlorobenzene (29–37 kJ/mol) over V_2O_5/TiO_2-based catalysts in the 200–400 °C temperature range [54], and those in the catalytic oxidation of 1,2-dichlorobenzene (34.4 and 31.5 kJ/mol) over V_2O_5/TiO_2 and V_2O_5/MoO_3–TiO_2 at temperature higher than 400 °C, respectively [55]. These comparisons demonstrated that the apparent activation energy of FeCa10 in this study is lower than those of reported catalysts.

3.6. In situ FTIR studies

In order to obtain more insight into the interfacial reaction in the decomposition of o-DCB, in situ FTIR measurements were carried out. FTIR spectra collected at different time intervals during o-DCB adsorption and oxidation over FeCa10 hollow microspheres at 250 °C are shown in Fig. 13a. FTIR spectra collected at different temperatures after 20 min reaction are shown in Fig. 13b. The band at 1459 cm^{-1} (νCOO^- asym), with an adjoining shoulder at 1432 cm^{-1} (νCOO^- sym), can be assigned to the carboxylates of the acetate type [56]. The weak peaks at 1585 (νCOO^- asym) indicate the formation of surface formate species [57]. The peaks at 2339 and 2361 cm^{-1} are ascribed to CO2 species [58]. As depicted in Fig. 13a, the intensities of the bands corresponding to surface carboxylates are markedly decreased after reaction for 10 min. A similar phenomenon is also observed with the increase of reaction temperature, shown in Fig. 13b, indicating the carboxylates are not the stable species in the oxidation process. These results could be due to the lower stability of these partial oxidation products and the increased catalytic activity of FeCa10 hollow microspheres at the higher temperature. Previous researches have proposed that the initial step in the catalytic oxidation chlorinated aromatics over V_2O_5/TiO_2 through a nucleophilic substitution process [59],
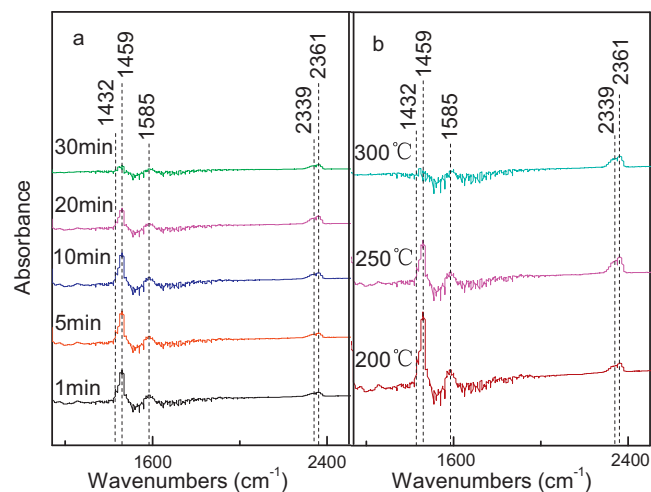

Fig. 13. In situ FTIR spectra of FeCa10 hollow microsphere collected (a) at 250 °C after 1, 5, 10, 20 and 30 min reaction and (b) at 200, 250 and 300 °C after 20 min reaction.

during which the chlorine atom is abstracted and replaced by a surface oxygen species, forming surface phenolates. In this case, no phenolate species was detected, instead, both types of carboxylates are observed even in the initial stage of the reaction at 250 °C, suggesting that the high activity of FeCa10 hollow microspheres is beneficial for the rapid decomposition of o-DCB. It can be seen that accompanying with the change of the concentration of carboxylates, the concentration of CO2 first increases, and then decreases. CO2 species is easily formed in the initial stage (1 min) and at lower temperature (250 °C) during the catalytic oxidation of o-DCB over FeCa10 hollow microspheres. It is noteworthy that no CO species is detected by the in situ FTIR spectroscopy, suggesting the high CO2 selectivity of FeCa10 hollow microspheres for catalytic oxidation of o-DCB. Given its excellent low-temperature activity, water-resistant performance, stability and lower apparent activation energy, FeCa10 hollow microspheres exhibit obvious advantage in the catalytic oxidation of Cl-VOCs.

4. Conclusions

Ca-doped FeO$_x$ hollow microspheres were synthesized and tested as catalysts for the oxidation of o-DCB in both the presence and absence of water. The optimal FeCa10 hollow microspheres (with 9.7 mol% Ca-doping) exhibited excellent catalytic activity, water-resistant performance, stability and CO2 selectivity. The apparent activation energy (21.6 kJ/mol) of optimal FeCa10 hollow microspheres is lower than the previous reports on the degradation of Cl-VOCs. The high activity of FeCa10 could be attributed to the small crystallite size, high surface active oxygen concentration, good low-temperature reducibility and synergic effect between CaO and Fe$_3O_4$. It is believed that the preparation approach for the Ca-doped FeO$_x$ hollow microspheres and the detailed discussion on the structure-reactivity relationship in this work can provide valuable knowledge on the development of novel, effective, environmentally friendly catalysts for the catalytic oxidation of toxic Cl-VOCs.

References

[1] K.L. Froese, O. Hutzinger, Environ. Sci. Technol. 30 (1996) 998–1008.
[2] J.R. González-Velasco, R. López-Fonseca, A. Aranzabal, J.I. Gutiérrez-Ortiz, P. Steltenpohl, Appl. Catal. B: Environ. 24 (2000) 233–242.
[3] C.M. Cooney, Environ. Sci. Technol. 35 (2001) 180A–181A.
[4] H. Duan, J. Li, Y. Liu, N. Yamazaki, W. Jiang, Environ. Sci. Technol. 45 (2011) 6322–6328.
[5] J.A. Conesa, L. Rey, S. Egea, M.D. Rey, Environ. Sci. Technol. 45 (2011) 5878–5884.
[6] Y. Fan, X. Lu, Y. Ni, H. Zhang, L. Zhao, J. Chen, C. Sun, Environ. Sci. Technol. 44 (2010) 3079–3084.
[7] Y. Fan, X. Lu, Y. Ni, H. Zhang, M. Zhu, Y. Li, J. Chen, Appl. Catal. B: Environ. 101 (2011) 606–612.
[8] Y. Dai, X. Wang, Q. Dai, D. Li, Appl. Catal. B: Environ. 111–112 (2012) 141–149.
[9] S. Lin, G. Su, M. Zheng, D. Ji, M. Jia, Y. Liu, Appl. Catal. B: Environ. 123–124 (2012) 440–447.
[10] S.H. Chang, K.H. Chi, C.W. Yong, B.Z. Hong, M.B. Chang, Environ. Sci. Technol. 43 (2009) 7523–7530.
[11] X. Wang, Q. Kang, D. Li, Appl. Catal. B: Environ. 86 (2009) 166–175.
[12] S. Albonetti, S. Blasioli, R. Bonelli, J.E. Mengou, S. Scirè, F. Trifirò, Appl. Catal. A: Gen. 341 (2008) 18–25.
[13] X. Ma, X. Feng, X. He, H. Guo, L. Lv, J. Guo, H. Cao, T. Zhou, Micropor. Mesopor. Mater. 158 (2012) 214–218.
[14] F. Wang, H. Dai, J. Deng, G. Bai, K. Ji, Y. Liu, Environ. Sci. Technol. 46 (2012) 4034–4041.
[15] X. Ma, Q. Sun, X. Feng, X. He, J. Guo, H. Sun, H. Cao, Appl. Catal. A: Gen. 450 (2013) 143–151.
[16] S. Lomnicki, B. Dellinger, Environ. Sci. Technol. 37 (2003) 4254–4260.
[17] A. Khaleel, A. Al-Nayli, Appl. Catal. B: Environ. 80 (2008) 176–184.
[18] H.C. Wang, H.S. Liang, M.B. Chang, J. Hazard. Mater. 186 (2011) 1781–1787.
[19] S.P. Decker, J.S. Klabunde, A. Khaleel, K.J. Klabunde, Environ. Sci. Technol. 36 (2002) 762–768.
[20] X. Ma, M. Zheng, W. Liu, Y. Qian, B. Zhang, W. Liu, J. Hazard. Mater. B127 (2005) 156–162.
[21] X. Ma, M. Zheng, W. Liu, Y. Qian, X. Zhao, B. Zhang, Chemosphere 60 (2005) 796–801.
[22] X. Ma, J. Shen, W. Pu, H. Sun, Q. Pang, J. Guo, T. Zhou, H. Cao, Appl. Catal. A: Gen. 466 (2013) 68–76.
[23] M. Tana, J. Zhang, H. Li, Y. Li, W. Li, Shen, Catal. Today 148 (2009) 179–183.
[24] X. Liu, J. Liu, Z. Chang, X. Sun, Y. L., Catal. Commun. 12 (2011) 530–534.
[25] C. Cavelius, K. Moh, S. Mathur, Cryst. Growth Des. 12 (2012) 5948–5955.
[26] L. Li, Y. Yu, F. Meng, Y. Tan, R.J. Hamers, S. Jin, Nano Lett. 12 (2012) 724–731.
[27] X. Qu, N. Kobayashi, T. Komatsu, ACS Nano 4 (2010) 1732–1738.
[28] T.P. Almeida, M. Fay, Y. Zhu, P.D. Brow, J. Phys. Chem. C 113 (2009) 18689–18698.
[29] X. Mou, Y. Li, B. Zhang, L. Yao, X. Wei, D. Su, W. Shen, Eur. J. Inorg. Chem. 2012 (2012) 2684–2690.
[30] W. Zhang, J. Chen, X. Wang, H. Qi, K. Peng, Appl. Organometal. Chem. 23 (2009) 200–203.
[31] Z. Wei, R. Xing, X. Zhang, S. Liu, H. Yu, P. Li, ACS Appl. Mater. Interfaces 5 (2013) 598–604.
[32] B. Rodríguez-González, F. Vereda, J.D. Vicente, R. Hidalgo-Álvarez, J. Phys. Chem. C 117 (2013) 5397–5406.
[33] P. Merchant, R. Collins, R. Kershaw, K. Dwight, A. Wold, J. Solid State Chem. 27 (1979) 307–315.
[34] O.B. Koper, I. Lagadic, A. Volodin, K.J. Klabunde, Chem. Mater. 9 (1997) 2468–2480.
[35] M. López Granados, M.D. Zafra Poves, D. Martín Alonso, R. Mariscal, F. Cabello Galisteo, R. Moreno-Tost, J. Santamaría, J.L.G. Fierro, Appl. Catal. B: Environ. 73 (2007) 317–326.
[36] A.P. Grosvenor, B.A. Kobe, M.C. Biesinger, N.S. McIntyre, Surf. Interface Anal. 36 (2004) 1564–1574.
[37] P.M. Rao, X. Zheng, Nano Lett. 11 (2011) 2390–2395.
[38] Y. Dai, X. Wang, D. Li, Q. Dai, J. Hazard. Mater. 188 (2011) 132–139.
[39] S. Minicò, S. Scirè, C. Crisafulli, R. Maggiore, S. Galvagno, Appl. Catal. B: Environ. 28 (2000) 245–251.
[40] S. Gaur, S. Johansson, F. Mohammad, C.S.S.R. Kumar, J.J. Spivey, J. Phys. Chem. C 116 (2012) 22319–22326.
[41] B.Y. Geng, J.Z. Ma, J.H. You, Cryst. Growth Des. 8 (2008) 1443–1447.
[42] S. Zhang, X. Zhao, H. Niu, Y. Shi, Y. Cai, G. Jiang, J. Hazard. Mater. 167 (2009) 560–566.
[43] M.V. Tsodikov, T.N. Rostovshchikova, V.V. Smirnov, O.I. Kiseleva, Y.V. Maksimov, I.P. Suzdalev, V.N. Ikorskii, Catal. Today 105 (2005) 634–640.
[44] S.C. Kim, W.G. Shim, Appl. Catal. B: Environ. 98 (2010) 180–185.
[45] C.E. Hetrick, F. Patcas, M.D. Amiridis, Appl. Catal. B: Environ. 101 (2011) 622–628.
[46] K. Poplawski, J. Lichtenberger, F.J. Keil, K. Schnitzlein, M.D. Amiridis, Catal. Today 62 (2000) 329–336.
[47] S. Krishnamoorthy, J.A. Rivas, M.D. Amiridis, J. Catal. 193 (2000) 264–272.
[48] Y. Liu, M. Luo, Z. Wei, Q. Xin, P. Ying, C. Li, Appl. Catal. B: Environ. 29 (2001) 61–67.
[49] J.R. González-Velasco, A. Aranzabal, J.I. Gutiérrez-Ortiz, R. López-Fonseca, M.A. Gutiérrez-Ortiz, Appl. Catal. B: Environ. 19 (1998) 189–197.
[50] J.R. González-Velasco, A. Aranzabal, R. López-Fonseca, R. Ferret, J.A. González-Marcos, Appl. Catal. B: Environ. 24 (2000) 33–43.
[51] R. López-Fonseca, A. Aranzabal, J.I. Gutiérrez-Ortiz, J.I. Álvarez-Uriarte, J.R. González-Velasco, Appl. Catal. B: Environ. 30 (2001) 303–313.
[52] R. López-Fonseca, J.I. Gutiérrez-Ortiz, J.R. González-Velasco, Appl. Catal. A: Gen. 271 (2004) 39–46.
[53] J.L. Shie, C.Y. Chang, J.H. Chen, W.T. Tsai, Y.H. Chen, C.S. Chiou, C.F. Chang, Appl. Catal. B: Environ. 58 (2005) 289–297.
[54] S. Krishnamoorthy, J.P. Baker, M.D. Amiridis, Catal. Today 40 (1998) 39–46.
[55] H.Y. Chang, S.P. Wang, J.R. Chang, H.S. Sheu, S.G. Shyu, Appl. Catal. B: Environ. 111–112 (2012) 476–484.
[56] B.H. Aristizabal, C.M. de Correa, A.I. Serykh, C.E. Hetrick, M.D. Amiridis, J. Catal. 258 (2008) 95–102.
[57] C.E. Hetrick, J. Lichtenberger, M.D. Amiridis, Appl. Catal. B: Environ. 77 (2007) 255–263.
[58] X. Ma, H. Sun, H. He, M. Zheng, Catal. Lett. 119 (2007) 142–147.
[59] J. Lichtenberger, M.D. Amiridis, J. Catal. 223 (2004) 296–308.